Trifluoromethanesulfonate (triflate) as a moderately coordinating anion: Studies from chemistry of the cationic coordinatively unsaturated mono- and diruthenium amidinates

Taizo Hayashida [a], Hideo Kondo [a], Jun-ichi Terasawa [a], Karl Kirchner [c], Yusuke Sunada [a,b], Hideo Nagashima [a,b,*]

[a] *Graduate School of Engineering Sciences, Kyushu University, Kasuga, Fukuoka 816-8580, Japan*
[b] *Institute for Materials Chemistry and Engineering, Kyushu University, Kasuga, Fukuoka 816-8580, Japan*
[c] *Institute of Applied Synthetic Chemistry, Vienna University of Technology, Getreidemarkt 9/163/AC, A-1060 Vienna, Austria*

Abstract

Triflate complexes of mono- and diruthenium amidinates, $(\eta^6\text{-}C_6R_6)Ru(\kappa^1\text{-}OTf)\{\eta^2\text{-}R'N=C(R'')NR'\}$ (**1**: R = Me; **2**: R = H) and $(\eta^5\text{-}C_5Me_5)Ru(\mu\text{-}\eta^2\text{-}{}^iPrN=C(Me)N^iPr)Ru(\kappa^1\text{-}OTf)(\eta^5\text{-}C_5R_5)$ (**3**: R = Me; **4**: R = H), are synthesized, and coordination behavior of the triflate anion to the coordinatively unsaturated ruthenium species is investigated by crystallography and variable temperature (VT) NMR spectroscopy (^{19}F, ^1H). The monoruthenium amidinate complexes have three-legged piano-stool structures in single crystals, which include a $\kappa^1\text{-}OTf$ ligand with the Ru–O bond of 2.15–2.20 Å. In contrast, reversible dissociation of OTf is observed in variable temperature ^1H NMR spectroscopy in liquid states; the activation energy for the dissociation and recombination of the OTf ligand is varied with the substituents on the arene and amidinate ligand in the corresponding ruthenium cation and the solvent used. A typical example of moderately coordinating ability of the OTf ligand is seen in ^{19}F NMR spectra of $(\eta^6\text{-}C_6Me_6)Ru(\kappa^1\text{-}OTf)\{\eta^2\text{-}{}^iPrN=C(Me)N^iPr\}$ (**1a**) and $(\eta^6\text{-}C_6H_6)Ru(\kappa^1\text{-}OTf)\{\eta^2\text{-}{}^iPrN=C(Me)N^iPr\}$ (**2a**) in CD_2Cl_2 at the temperature range from −90 to 20 °C, in which the OTf anion is dissociated in **1a**, whereas **2a** has a relatively robust Ru–OTf bond. Combination of crystallography and VT NMR contributes to understanding the difference in coordination behavior of the OTf ligand between two diruthenium amidinates, $(\eta^5\text{-}C_5Me_5)Ru(\mu\text{-}\eta^2\text{-}{}^iPrN=C(Me)N^iPr)Ru(\kappa^1\text{-}OTf)(\eta^5\text{-}C_5Me_5)$ (**3**) and $(\eta^5\text{-}C_5Me_5)Ru(\mu\text{-}\eta^2\text{-}{}^iPrN=C(Me)N^iPr)Ru(\kappa^1\text{-}OTf)(\eta^5\text{-}C_5H_5)$ (**4**); the results suggest that the electron-donating and sterically demanding $\eta^5\text{-}C_5Me_5$ helps for dissociation of the triflate ligand. Moderate coordinating ability of the triflate anion sometimes provides characteristic reactions of mono- and diruthenium amidinates which differ from the corresponding neutral halogeno-compounds or cationic coordinatively unsaturated homologues bearing fluorinated tetraarylborates; a typical example is given by inhibition of coordination of ethylene to the $[(\eta^6\text{-}C_6H_6)Ru\{\eta^2\text{-}{}^tBuN=C(Ph)N^tBu\}]^+$ species by the OTf ligand.
© 2006 Elsevier B.V. All rights reserved.

Keywords: Ruthenium amidinate; Triflate; Coordinatively unsaturated

1. Introduction

Importance of weakly coordinating anions in organometallic chemistry has been widely recognized in a number of review articles, which covers fundamentals in coordination behavior of classical "weakly coordinating" anions such as ClO_4^-, PF_6^-, and BF_4^- and non-classical "larger and more weakly coordinating" anions such as fluorinated tetraarylborates, anionic methylaluminoxane, and carborane anions [1]. This area has lately expanded to homogeneous catalysis; in particular, their deep knowledge is necessary for developing new metallocene catalysts for industrially important olefin polymerization processes [2]. Trifluoromethanesulfonate (triflate; $CF_3SO_3^-$; TfO^-) has long been believed as a classical "non-coordinating" anion, and in

* Corresponding author. Tel./fax: +81 925837819.
  E-mail address: nagasima@cm.kyushu-u.ac.jp (H. Nagashima).

fact, many transition metal triflates act as a cationic coordinatively unsaturated species, which allow facile coordination of other auxiliary ligands such as water, pyridine, and phosphines to result in throwing away the triflate anion out of the coordination sphere: $M–OTf + L \rightarrow M(L)^+ (OTf)^-$. However, it has been recognized that triflate has relatively strong coordinating ability to the metal center similar to ClO_4^- compared with PF_6^-, BF_4^-, and fluorinated tetraarylborates; many complexes having metal–OTf bonds have been isolated and characterized [1]. The progress in understanding the weakly coordinating anions has given unique insights in differences in the coordination behavior among both classical and non-classical weakly coordinating anions; for example, chemistry of transition metal Lewis acids has provided catalysis for asymmetric Diels–Alder reactions, of which rate and selectivity are dependent on the weakly coordinating counter anions used [3]. In this context, systematic studies on the organometallic chemistry of weakly coordinating anions bound to a series of cationic transition metal species with similar structures should be important for understanding the effect of weakly coordinating anions; in particular, triflate having a relatively strong coordination ability compared with other weakly coordinating anions is of interest to be investigated.

Chemistry of κ^1-OTf complexes of ruthenium has received considerable attention of organometallic chemists since mid 90s; molecular structures of several complexes have been published, and discussion on a possible existence of κ^1-OTf species in solution was performed using NMR techniques [4]. A typical example is [Ru(OTf)(6′-diphenylphosphino-1-naphthyl)(PPh$_2$OH)]OTf [4h], of which crystallography showed existence of two triflates; one is bonded to the ruthenium center with the Ru–O bond distance of 2.155(4) Å, whereas the other is out of the coordination sphere. Two distinct ^{19}F signals due to the triflates are seen at room temperature; one is assigned to the κ^1-OTf (δ −78.2), whereas the other is due to the $^-$OTf (δ −79.5) in CD$_2$Cl$_2$. In many other κ^1-OTf ruthenium complexes, the Ru–O bond distance in the crystal structures is ca. 2.15–2.25 Å, the ^{19}F resonance in solution appears in lower fields than that of the free $^-$OTf [4]. Although these data indicate that the triflate anion is tightly bound to the cationic ruthenium center, treatment of the κ^1-OTf ruthenium complexes with several donor ligands result in their coordination to the cationic ruthenium center accompanied by movement of the triflate out of the coordination sphere. These are good examples suggesting the triflate is a moderately weak coordinating anion to the cationic ruthenium species; the Ru–O interaction is strong enough to detect by crystallography and ^{19}F NMR spectroscopy but weak enough to react with other ligands.

We are interested in coordination chemistry of triflate from the side of cationic ruthenium species. When we consider the dissociation (or solvent-assisted dissociation) of the M–OTf bond, an important factor should be stability of cationic species M$^+$, which may exist as the coordin-

Fig. 1. Triflate complexes of ruthenium amidinates.

atively unsaturated form in less-polar solvents: M–OTf $\leftrightarrow$ M$^+$ + $^-$OTf. The equilibrium would shift to the right side, when M$^+$ is stable. If not very stable, the equilibrium should be favored for the left side, so that the unstable M$^+$ is protected by bonding with $^-$OTf. Our cationic coordinatively unsaturated ruthenium amidinate complexes are good candidates to discuss about the triflate chemistry from this side [5]. Coordinatively unsaturated yet isolable cationic ruthenium complexes, [(η^6-C$_6$R$_6$)-Ru{η-R′N=C(R″)NR′}]$^+$X$^-$ (R = Me, H, X = PF$_6$, BF$_4$, TFPB), were synthesized from the corresponding neutral halogeno complexes [5b]. In contrast to the three-legged piano-stool structures of the halogeno-precursors [6], center of the C$_6$Me$_6$ ligand, the ruthenium atom, and the two nitrogen atoms are in a plane in the molecular structure of [(η^6-C$_6$Me$_6$)Ru{^{i}PrN=C(Me)N^{i}Pr}]$^+$PF$_6^-$, and possible interaction of the central carbon of the amidinate ligand to the ruthenium center is indicative of π-stabilization to compensate the coordinative unsaturation. Coordinatively unsaturated diruthenium amidinates, [(η^5-C$_5$Me$_5$)-Ru(μ-η^2-^{i}PrN=C(Me)N^{i}Pr)Ru(η^5-C$_5$R$_5$)]$^+$X$^-$ (R = H, Me; X = TFPB, PF$_6$, BF$_4$, etc.), are also synthesized from the corresponding halogeno-precursors, and crystallographic studies showed that the molecular structures of [(η^5-C$_5$Me$_5$)Ru(μ-η^2-^{i}PrN=C(Me)N^{i}Pr)Ru(η^5-C$_5$Me$_5$)]$^+$X$^-$ differ from the corresponding halogeno-precursors [5c,5d]. The aim of this paper is preparation and characterization of triflate complexes of these coordinatively unsaturated ruthenium amidinates, 1–4 (Fig. 1). As indicated from the moderate coordination ability of triflate, the OTf is bonded to the ruthenium center in crystal structures. In contrast, solution dynamics in ^{1}H and ^{19}F NMR spectroscopy indicates how facile is the dissociation of the OTf, that depends on the nature of the ruthenium cation. The moderate coordination ability also affects the reactivity of the triflate complexes, which sometimes differs from both the neutral halogeno-precursor and the cationic coordinatively unsaturated complexes.
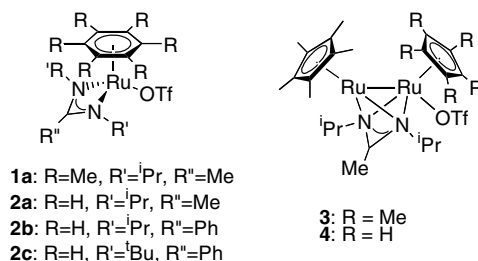
2. Results and discussion

2.1. Synthesis and the molecular structures of triflate complexes of mono- and diruthenium amidinates

Triflate complexes of monoruthenium amidinates, (η^6-C$_6$R$_6$)Ru(κ^1-OTf){η^2-R′N=C(R″)NR′} (**1a**, **2a**, **2b**, and

2c; see Fig. 1) were synthesized from the corresponding halogeno-precursors, $(\eta^6\text{-}C_6R_6)Ru(X)\{\eta^2\text{-}R'N=C(R'')NR'\}$ (**5**, **6**), by treatment with AgOTf in CH_2Cl_2. The diruthenium amidinates, $[(\eta^5\text{-}C_5Me_5)Ru(\mu\text{-}\eta^2\text{-}{}^iPrN=C(Me)N^iPr)\text{-}Ru(\eta\text{-}OTf)(\eta^5\text{-}C_5Me_5)]$ (**3**) and $[(\eta^5\text{-}C_5Me_5)Ru(\mu\text{-}\eta^2\text{-}{}^iPrN=C(Me)N^iPr)Ru(\eta\text{-}OTf)(\eta^5\text{-}C_5H_5)]$ (**4**; R = H), were prepared from the corresponding halogeno-precursors by treatment with AgOTf and TlOTf, respectively. As reported previously, the TFPB homologues of these triflate complexes are coordinatively unsaturated, showing intense blue to violet color [5b]. In contrast, the halogeno-homologues of these complexes are orange or red and neutral. From X-ray structure determination of several mono- and diruthenium amidinates, these coordinatively saturated and unsaturated complexes can typically be illustrated as shown in Fig. 2, where the angle θ is defined by the centroid of the ring (the arene or cyclopentadienyl ring)—the Ru atom with the plane consisting of the two nitrogen atoms of the amidinate ligand and the ruthenium atom. It is clearly seen from the value of θ that the coordinatively saturated monoruthenium amidinates **A** have typical three-legged piano-stool structures (θ = ca. 145°) [6,7] (structural details of **9-OTf** and **10-OTf** are discussed later), whereas the coordinatively unsaturated analogue **B** is a two-legged piano-stool (θ = 174°) [5]. Structural features of diruthenium amidinates are similar to those of monoruthenium amidinates; one of the ruthenium atoms is close to **A** with three-legged piano-stool structures in the coordinatively saturated **C** (θ = 156–160°), whilst those of the coordinatively unsaturated analogues **D** are close to **B** with two-legged piano-stool structures (θ = 172–174°).

The molecular structures of **1a**, **3**, and **4** were determined by crystallography. A single crystal suitable for X ray structure determination of **2a** was unfortunately not obtained; however, its molecular structure is believed to be similar

to that of the analogous compound **2c**. The ORTEP drawings (Fig. 3) revealed that the ligand arrangement around the ruthenium is similar to that seen in the coordinatively saturated halogeno-analogues; this is clearly demonstrated by the angle θ [148.9° (**1a**), 138° (**2c**), 160.3° (**3**), and 154.9° (**4**)]. The Ru–O bond distance is another indication of coordinatively unsaturated nature, though the crystallography contains some influence of crystal packing. However, comparison in the bond distances and angles among the molecules with similar structures seems to have some sense for discussion. The three-legged piano-stool structures of **1a** and **2c**, suggest the coordinative saturation by the tightly bound OTf ligand; however, the longer Ru–O bond of **1a** [2.199(3) Å] may suggest the weaker Ru–O interaction than that seen in **2c** [Ru–O = 2.155(5) Å]. The electron-donating property of the C_6Me_6 ligand in **1a** possibly contribute to stabilizing the coordinatively unsaturated ruthenium cation, giving the weaker Ru–O interaction. The diruthenium amidinate **4** has a slightly longer Ru–O bond distance [Ru–O = 2.213(5) Å] than those seen in **1a** and **2c**, suggesting the coordinatively saturated nature in a single crystal. In sharp contrast, **3** has a significantly longer Ru–O distance (2.360(2) Å), and relatively large Ru–O–S angle (150.63°). These suggest that **3** may have some coordinatively unsaturated nature even in a single crystal. This is inconsistent with the angle θ not close to those of $[(\eta^5\text{-}C_5Me_5)Ru(\mu\text{-}\eta^2\text{-}{}^iPrN=C(Me)N^iPr)Ru(\eta^5\text{-}C_5Me_5)]^+Y^-$ [Y = PF_6, $B(C_6F_5)_4$], but in accord with an intense purple color of **3** in solid states. Steric circumstances in **3**, in which the bulky C_5Me_5 group and isopropyl moieties interfere the coordination of OTf, is one explanation of this unusual bond distance and angle, whereas electron-donation by the C_5Me_5 groups is another reason. In a similar crystal structure reported in *trans*-$[Ru(OTf)(CN)(dppe)_2]$ having a long Ru–O distance of 2.410(5) Å and large Ru–O–S angle (160.5(3)°), strong trans-influence of the CN ligand and steric circumstances are discussed as the possible explanation [4l] (Tables 1 and 2).

In summary, the data of the angle θ suggests that the triflate ligand has relatively strong coordinating ability to give the crystal structures close to the neutral halogeno-homologues, whereas electronic and steric circumstances provide the variation of the Ru–OTf interaction, which is estimated from the Ru–O bond distance of each complex.

2.2. Variable temperature NMR studies of triflate complexes of mono- and diruthenium amidinates

In contrast to the crystal structures suggesting the coordinatively saturated nature in solid states, it is known that solution dynamics measured by variable temperature NMR spectroscopy can predict the coordinating ability of OTf in liquid states. There are several factors which affect the solution dynamics, steric and electronic properties of the auxiliary ligands, e.g. C_6H_6 vs. C_6Me_6 (**1** vs. **2**), C_5Me_5 vs. C_5H_5 (**3** vs. **4**), and substituents of the amidinate ligands (**2**), and the polarity and coordinating ability
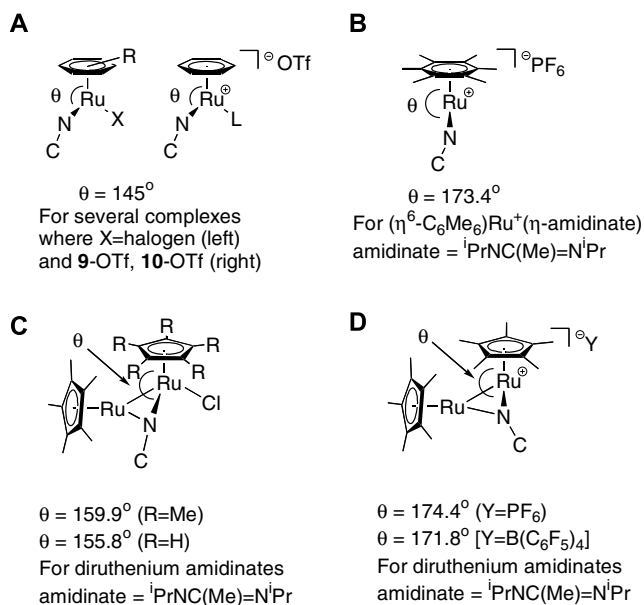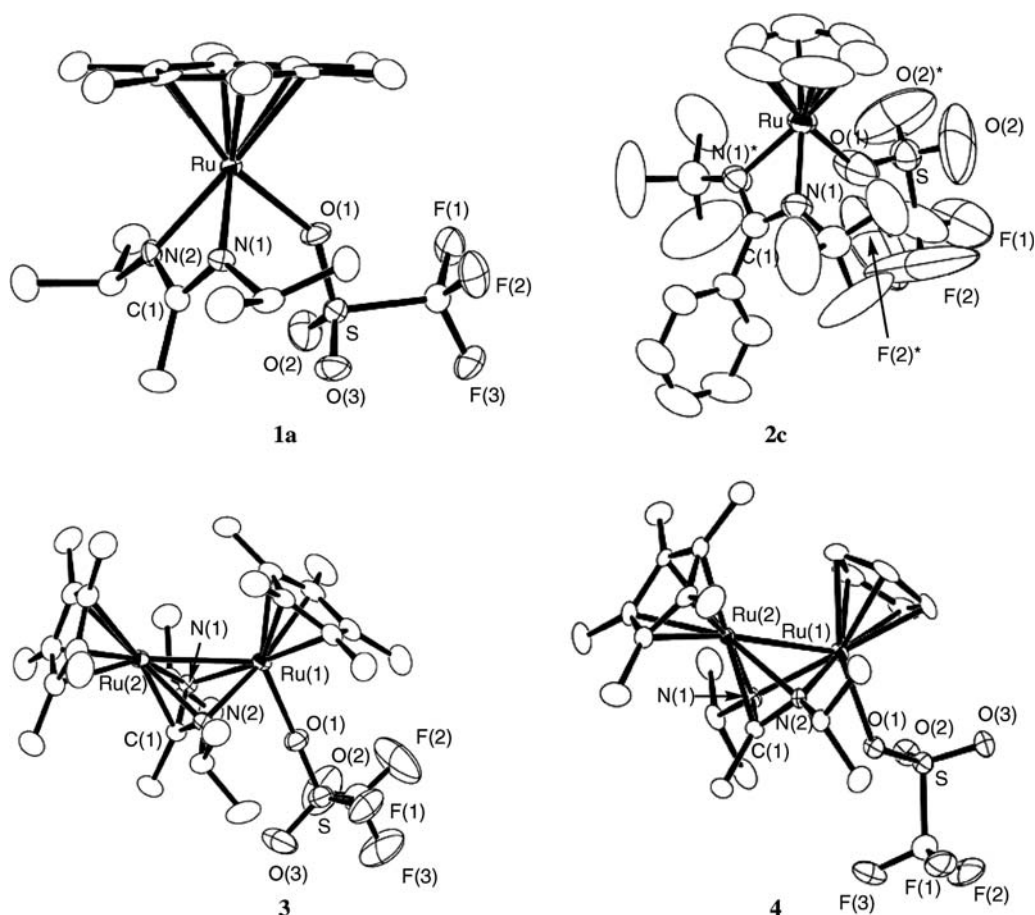

Fig. 2. Dihedral angles θ.

Fig. 3. The ORTEP drawings of **1a**, **2c**, **3**, and **4**.

Table 1
Representative bond distances (Å) and angles (°) of monoruthenium amidinates, **1a**, **2c**, **9-OTf**, and **10-OTf**

	1a	**2c**	**9-OTf**	**10-OTf**
Bond distances (Å)				
Ru–O(1)	2.199(3)	2.155(5)		
Ru–N(3)			2.151(4)	
Ru–C(2)				1.956(4)
Ru–N(1)	2.112(4)	2.083(3)	2.092(3)	2.093(3)
Ru–N(2)	2.112(4)	2.083(3)	2.122(4)	2.087(4)
Ru–C(1)	2.546(5)	2.55(3)	2.561(3)	2.57(3)
C(2)–N(3)				1.151(6)
Ru–C$_6$ ring (centroid)	1.678(3)	1.662(1)	1.7475(3)	1.704(1)
N(1)–C(1)	1.329(8)	1.318(5)	1.328(5)	1.318(5)
N(2)–C(1)	1.324(7)	1.318(5)	1.327(5)	1.328(5)
Bond angles (°)				
N(1)–Ru–N(2)	62.1(2)	61.9(2)	61.9(1)	62.0(1)
N(1)–Ru–O(1)	86.5(2)	81.2(2)		
N(2)–Ru–O(1)	87.0(2)	81.2(2)		
N(1)–Ru–N(3)			87.4(2)	
N(2)–Ru–N(3)			84.3(1)	
N(1)–Ru–C(2)				85.5(2)
N(2)–Ru–C(2)				86.0(2)
N(1)–C(1)–N(2)	110.4(5)	108.6(5)	109.5(4)	108.9(4)

Table 2
Representative bond distances (Å) and angles (°) of diruthenium amidinates **3** and **4**

	3	**4**
Bond distances (Å)		
Ru(1)–Ru(2)	2.9135(2)	2.7589(5)
Ru(1)–O	2.360(2)	2.213(3)
Ru(1)–R^1	1.7926(2)	1.7899(4)
Ru(2)–R^2	1.8320(2)	1.7998(4)
Ru(1)–N(1)	2.133(2)	2.116(3)
Ru(1)–N(2)	2.132(2)	2.119(3)
Ru(2)–N(1)	2.092(2)	2.091(3)
Ru(2)–N(2)	2.122(3)	2.098(3)
Ru(2)–C(1)	2.125(3)	2.131(4)
N(1)–C(1)	1.381(4)	1.372(5)
N(2)–C(1)	1.379(4)	1.378(5)
Bond angles (°)		
θ_1	161.81(4)	154.71(6)
θ_2	123.95(4)	115.06(7)
θ_3	118.80(7)	125.07(9)
N(1)–Ru(1)–O(1)	79.22(9)	81.5(1)
N(2)–Ru(1)–O(1)	84.95(8)	81.3(1)
N(1)–Ru(1)–N(2)	61.48(9)	61.4(1)
N(1)–C(1)–N(2)	104.3(2)	103.7(3)

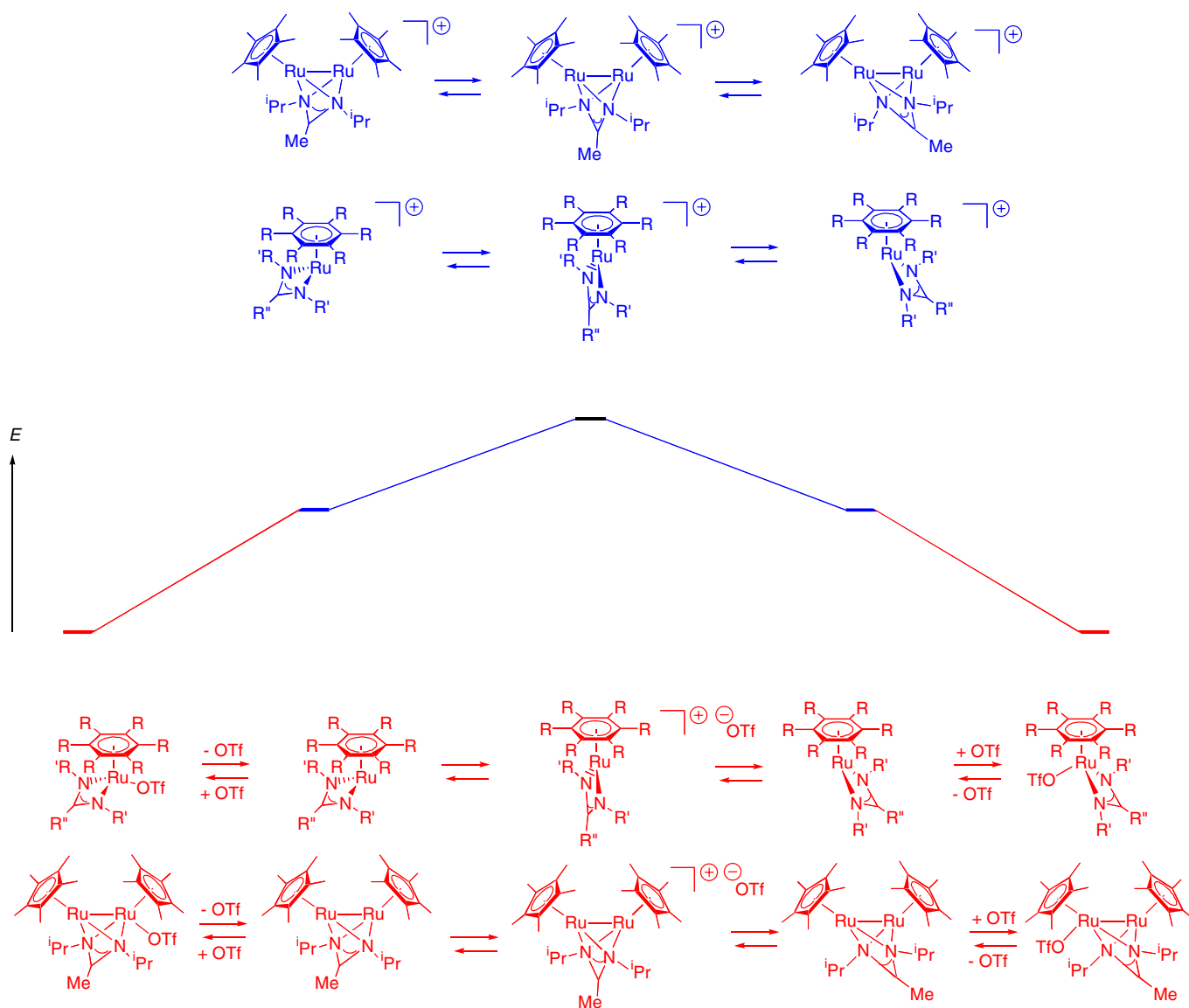R^1 = center of Cp or Cp*
R^2 = center of Cp*
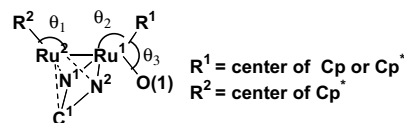
Fig. 4. Simplified schemes for flipping of the amidinate ligand in coordinatively unsaturated complexes vs. triflate complexes. A possibility that the cationic species may be stabilized by solvation or coordination of the solvents is not taken into consideration in these schemes for clarity.

of the solvent used. An advantage of the mono- and diruthenium amidinates **1**–**4** is that coordinatively unsaturated cationic ruthenium species formed by dissociation of ⁻OTf are stable enough to isolate as the TFPB anion. As discussed in our previous papers [5a,5b,5c,5d], the amidinate ligands of all of these coordinatively unsaturated TFPB complexes potentially show dynamic behavior as shown in Fig. 4 (blue scheme),[1] in which the flipping of the amidinate ligand leads to conversion of a pseudo-three-legged piano-stool form to the other through the transition state with a two-legged piano-stool structure. In fact, variable temperature ¹H NMR spectroscopy of the TFPB homologues of **1**, **2**, and **3** showed rapid flipping of the amidinate ligand, in which the activation energy is low enough to pre-

vent the flipping even below −78 °C. The crystal structures suggesting the coordination of the OTf ligand to **1**, **2**, and **3** indicate that the coordination may stabilize the pseudo-three-legged form. Thus, the flipping of the amidinate ligand takes place from the κ^1-OTf three-legged piano-stool form to its enantiomer through a cationic two-legged piano-stool transition state; this provides substantial increase of activation energy for as shown in Fig. 4 (red scheme). In other words, solution dynamics of ¹H NMR of the triflate homologues of **1**, **2**, and **3** may provide good evidence that the OTf ligand interferes the flipping of the amidinate ligand by coordination.

¹H NMR studies on **1a**, **2a** and **2b** clearly showed that the OTf ligand prevents the flipping at low temperatures. A typical example for the dynamism is seen in the diastereotopic Me signals of isopropyl group on the amidinate ligand in **2a** in ¹H NMR spectrum (Scheme 1). In CD₂Cl₂,

---

[1] For interpretation of the references in color in Fig. 4, the reader is referred to the web version of this article.
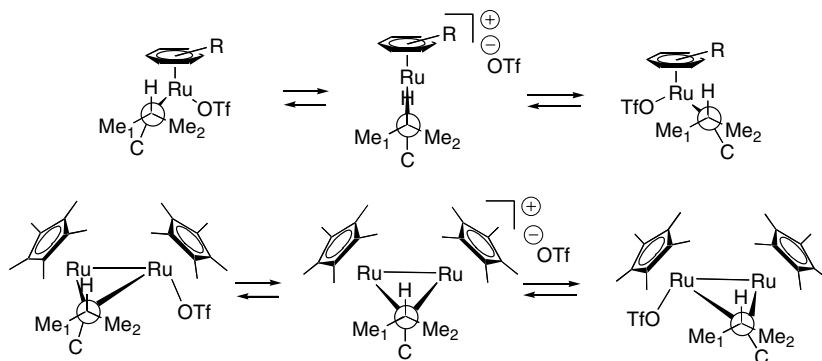
Scheme 1. Dynamisms of the isopropyl group.

two methyl signals appeared independently at −90 °C, coalesced at −30 °C, and became a single doublet at 25 °C (Fig. 5). Similar spectral change was seen at 20, 40, and 80 °C, respectively, in toluene-d_8. These are due to reversible coordination of OTf providing the flipping of the amidinate ligand as shown in Scheme 1; the calculated ΔGs are dependent on the solvent used, 11.4 (CD_2Cl_2) and 15.7 (toluene-d_8) kcal/mol (Table 3). Similar experiments on 1a and 2b revealed that ΔG is dependent on the substituents on the arene ring [$\Delta G(\eta^6\text{-}C_6H_6) > \Delta G(\eta^6\text{-}C_6Me_6)$], those of the amidinate group [$\Delta G(\eta\text{-}^iPrNC(Ph)N^iPr) > \Delta G(\eta\text{-}^iPrNC(Me)N^iPr)$]. As discussed in the first paper showing evidence of the coordinating ability of triflate to ruthenium, the cationic ruthenium species formed by dissociation of OTf is possibly stabilized by the solvent. In extreme cases using polar and coordinating solvents, dissociation of OTf are assisted by coordination of the solvent, whereas dissociation of OTf occurs spontaneously and the solvent plays a small role for the stabilization of the cationic species in the other cases using less-polar and weakly coordinating solvents. The difference in ΔG between that in CD_2Cl_2 and in toluene-d_8 may reflect polarity and coordinating ability of CD_2Cl_2 to the ruthenium cation. The result of $\Delta G(\eta^6\text{-}C_6H_6) > \Delta G(\eta^6\text{-}C_6Me_6)$ can be explained by stabil-

ization of the cationic coordinatively unsaturated ruthenium species by more electron-donating $\eta^6\text{-}C_6Me_6$ ligand. The stabilized ruthenium cation does not need further stabilization by coordination of OTf. The result of $\Delta G(\eta\text{-}^iPrNC(Ph)N^iPr) > \Delta G(\eta\text{-}^iPrNC(Me)N^iPr)$ may be attributed to bulkiness of the phenyl group in 2b compared with the methyl group in 2a, which protect the coordinatively unsaturated ruthenium center from the coordination of OTf. Resonance stabilization by the phenyl group is difficult to consider, because the crystal structure of 2c suggests that the phenyl group of 2b is perpendicular to the amidinate plane.

Table 3
The coalescent temperature on the ^1H NMR and the calculated activation energy of the reversible coordination of the triflate to $[(\eta^6\text{-}C_6R_6)Ru(\eta^2\text{-}amidinate)]^+$

Complex	In CD_2Cl_2		In toluene-d_8	
	Coalescent temperature (°C)	$\Delta G^{\ddagger}$ (kcal/mol)	Coalescent temperature (°C)	$\Delta G^{\ddagger}$ (kcal/mol)
1a	< −100	Not determined	0	13.0
2a	−30	11.4	40	15.7
2b	> 40	Not determined	100	18.6
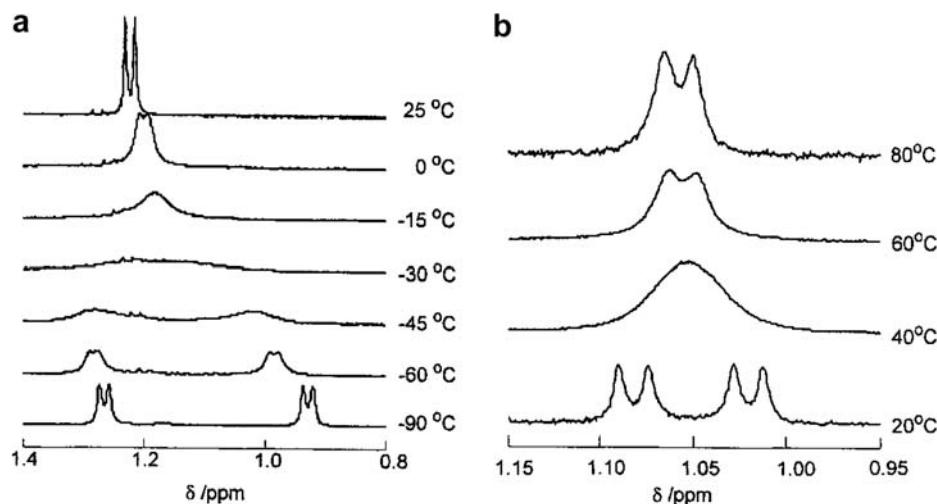
Fig. 5. Variable temperature ^1H NMR signals for diastereotopic Me protons of the N–^iPr group of 2a in CD_2Cl_2 (left) and in toluene-d_8 (right).

The effect of the arene ring between **1a** and **2a** was further investigated by variable temperature ^{19}F NMR. In several earlier reports are discussed chemical shifts of ^{19}F resonances due to the coordinated and uncoordinated triflate ligand: the latter appears around −79 ppm in CD_2Cl_2, and the former is observed at downfield by 1–2 ppm. A single ^{19}F peak was seen at −78.95 ppm for **1a** at room temperature; no spectral change was observed even at −90 °C. In contrast, **2a** provided a single ^{19}F signal at room temperature at −77.25 ppm; a small broad peak appeared at −78.1 ppm below −50 °C, which became sharp as the temperature down to −70 °C. The peak ratio of the former (−77.25) to the latter (−78.1) is 9:1. We consider the new peak at −78.1 ppm to be uncoordinated ⁻OTf, which is in equilibrium with the coordinated OTf seeing at −77.25 ppm. Thus, the triflate is uncoordinated in a CD_2Cl_2 solution of **1a**, whereas that is mainly coordinated and only partly dissociated in that of **2a**. This is consistent with $\Delta G(\eta^6\text{-}C_6H_6) > \Delta G(\eta^6\text{-}C_6Me_6)$.

Similar NMR experiments were done with diruthenium amidinates **3** and **4**. Although the μ-amidinate ligand in **4** does not show any dynamic behavior, that in **3** and its TFPB homologue is rapidly flipping in solution. Variable temperature ^{19}F NMR of **3** in CD_2Cl_2 showed only a signal due to the uncoordinated OTf, whereas that of **4** provide a major and minor peak at −78.2 and −79.3 ppm, respectively, below −20 °C, suggesting that the triflate is mainly coordinated and partly dissociated. The results can be explained by better donor property and steric bulkiness of the C_5Me_5 ligand in **3**, which give favorable influence for the stabilization of cationic coordinatively unsaturated diruthenium amidinate species.

2.3. Representative reactions showing the moderate coordinating ability of ⁻OTf

As described above, the crystal structures and solution dynamics of the triflate complexes of mono- and diruthenium amidinates indicate that the triflate anion is coordinated in a κ¹-mode in solid states, whereas it reversibly dissociates in liquid states. Of importance is how easy is the dissociation, which apparently depends on the elec-

tronic nature and steric circumstances of the corresponding coordinatively unsaturated cationic species. Among the triflates we examined, the complexes, $(\eta^6\text{-}C_6H_6)Ru(\kappa^1\text{-}OTf)\{\eta^2\text{-}R'N=C(R'')NR'\}$ **2a**, **2b**, and **2c**, have the most strongly bound OTf ligand to the ruthenium center; this is evidenced by ^{19}F resonance assignable to the coordinated triflate at the temperature range from 20 to −70 °C. VT-^{1}H NMR also supports this. The relatively strong coordination of triflate to the metal center in **2a**–**2c** may provide different reactivity of **2a**–**2c** with auxiliary ligands from that of the corresponding coordinatively unsaturated TFPB homologues. For the examination of this, we carried out the reactions of several ligands with **2c**.

As described in our previous paper, $[(\eta^6\text{-}C_6H_6)Ru\{\eta^2\text{-}{}^tBuN=C(Ph)N^tBu\}]^+(TFPB)^-$ (**7**) showing intense blue color reacted with PPh_3, pyridine, CN^tBu, CO, and $CH_2=CH_2$ to give the corresponding adducts almost instantly [5b]. The reactivity of **2c** was smaller than **7**. As shown in Scheme 2, PPh_3, pyridine, and CN^tBu reacted smoothly with **2c** to give the corresponding adducts, whereas treatment of CO with **2c** results in decomposition of the product (vide infra). The products were characterized by spectroscopic methods, and X-ray structure determination of two of the compounds, **9-OTf** and **10-OTf**, showed their three-legged piano-stool structures (Fig. 6). Of importance is the reaction of **2c** with ethylene having the weakest donor property among we examined, which afforded no adduct. In other words, ⁻OTf is a stronger ligand than ethylene to $[(\eta^6\text{-}C_6H_6)Ru\{\eta^2\text{-}{}^tBuN=C(Ph)N^tBu\}]^+$; ethylene cannot replace the triflate on the ruthenium center due to the weak coordination ability. This clearly demonstrates moderately weak coordinating ability of triflate, which differs from other weakly coordinated anions. There are number of reports suggesting differences in reactivity between transition metal halide complexes and their triflate homologues, which are classified into "neutral" and "cationic", respectively; the former is less reactive than the latter. In fact, we have preliminary results showing that the reactions of neutral halogeno-homologues of **2** with pyridine, CO, and $CH_2=CH_2$ gave no adduct, though the adduct formation was detectable by NMR in the reactions with PPh_3
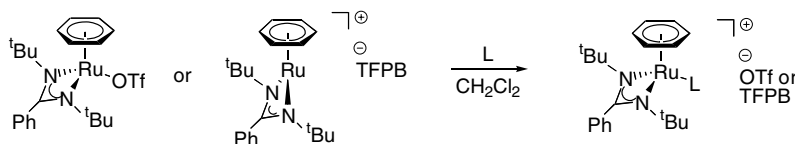
L	the OTf complex (**2c**)	the TFPB homologue[b]
PPh_3	94%	84%
pyridine	82%	98%
${}^tBuNC$	89%	98%
CO	decomposed	90%
ethylene	No reaction	60%

a. Isolated yields are listed. b. see ref 5b.

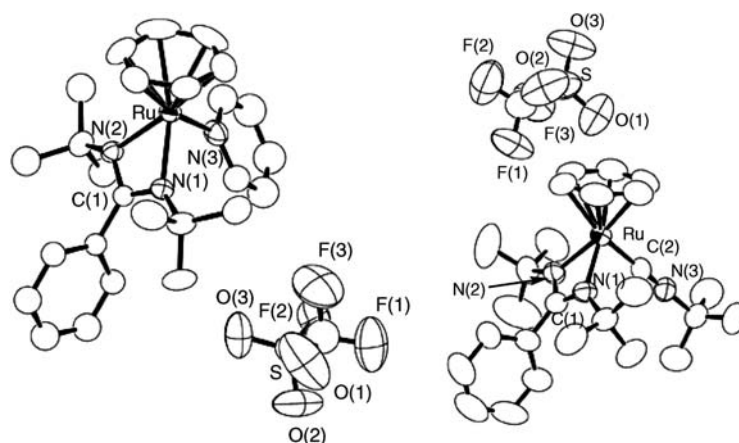Scheme 2. Reaction of **2c** and its TFPB homologue with auxiliary ligands.

Fig. 6. The molecular structures of **9-OTf** (left) and **10-OTf** (right).

and CN^{t}Bu [6c]. In contrast to this, the reactivity difference between the triflate complexes and their TFPB homologues, which are both classified into the "cationic complexes" has not been fully investigated in organometallilc chemistry yet. The above results clearly showing the reactivity order of [Ru]$^+$[TFPB]$^-$ > [Ru]$^{\delta+}$[OTf]$^{\delta-}$ > Ru–X, are one of the rare example demonstrating the moderately weak coordinating ability of the triflate anion.

3. Conclusion

Cationic transition metal species plays an important role in some of the homogeneous catalysis, and it has become popular that coordinating ability of the corresponding counter anion sometimes affects the catalytic activity and selectivity [2,3]. Such counter anion effect is well investigated in highly oxophilic cationic early transition metal complexes [2], in particular, in terms of mechanisms for olefin polymerization by metallocene catalysts; however, less oxophilic late transition metal cations have relatively been ill investigated [3]. Among studies on the triflate complexes of ruthenium, which mainly dealt with crystal structures and spectroscopy, the present report is unique to let the readers understand how the triflate is bound to the metal center from both crystal structures, solution dynamics, and reactions with auxiliary ligands. The particular uniqueness is attributed to the cationic mono- and diruthenium amidinates **1–4**, which can be isolated as coordinatively unsaturated forms by using TFPB as the counter anion. In this context, comparison in the structures, dynamics, and reactions between the triflate complexes **1–4** with their TFPB homologues, as well as that between the triflate complexes with coordinatively saturated halogeno-homologues, provides many clues for understanding the coordinating ability of the triflate anion, which apparently differs from both halides and TFPB. The results described in this paper clearly demonstrated the nature of the triflate anion as a moderately coordinating anion, which facilely dissociates from the metal center when the counter cationic species is stabilized by electronic or steric reasons; these are seen in the complexes **1** and **3**. In con-

trast, the complexes which are not well stabilized by the auxiliary ligands require the tight coordination of the triflate for the stabilization of the complexes; these are visible in the complexes **2** and **4**. In the extreme case, the triflate tightly bound to the ruthenium inhibits its replacement by a weak ligand, ethylene; this clearly predicts that use of the triflate should be careful when the homogeneous catalysis include cationic ruthenium intermediates and activation of weakly coordinating substrates such as olefins. These aspects have first been provided by nice contribution of organometallic chemistry of coordinatively unsaturated ruthenium amidinates, and would contribute to chemistry of the weakly coordinating anion from fresh insights.

4. Experimental

4.1. General methods

Manipulation of air- and moisture sensitive organometallic compounds was carried out under a dry argon atmosphere using standard Schlenk techniques associated with a high-vacuum line and a nitrogen-filled glove-box. All solvents were distilled over appropriate drying reagents prior to use (toluene, pentane, Et$_2$O; Ph$_2$CO/Na:MeCN, CH$_2$Cl$_2$; CaH$_2$:acetone; MS4A). ^{1}H, ^{13}C, ^{19}F, and ^{31}P NMR spectra were recorded on a JEOL Lambda 400 or 600 MHz spectrometer. The chemical shifts were recorded in ppm relative to the solvent signal or standard references (^{19}F; external C$_6$F$_6$, ^{31}P; external 85% H$_3$PO$_4$). IR spectra were measured on a JASCO FT/IR-550 spectrometer. Melting points were measured on a Yanaco micromelting point apparatus. ESI mass spectra were recorded on a JEOL JMS-T100CS spectrometer. Elemental analyses were preformed by the Elemental Analysis center, Faculty of Science, Kyushu University.

4.2. Preparation of (η^6-C$_6$R$_6$)Ru(κ^1-OTf){η^2-R'N=C(R'')NR'} (1a, 2a, 2b, and 2c)

The triflates of monoruthenium amidinates, **1a**, **2a**, **2b**, and **2c**, were prepared by treatment of AgOTf with the

corresponding halogeno-precursors, **5a-Br**, **6a-Br**, **6b-Cl**, and **6c-Cl**, respectively. In a typical example, the complex **6c-Cl** (69 mg, 0.16 mmol) and AgOTf (41 mg, 0.16 mmol) were dissolved in CH_2Cl_2 at $-78\,°C$. The mixture was slowly warmed to room temperature, and stirred for 1 h. Insoluble AgCl was filtered off, and the filtrate was concentrated. The crude product was recrystallized from a mixture of CH_2Cl_2 and pentane at $-35\,°C$ to give **2c** as air-sensitive red-orange crystals (58 mg, 0.10 mmol, 67%).

1a: yield 64%, mp 148 °C (dec). ESI-TOF: M−⁻OTf: 405.18. Exact mass (ESI-TOF): Calcd. for $^{12}C_{20}{}^{1}H_{35}$-$^{14}N_2{}^{102}Ru_1$: 405.1844. Found: 405.1845. ¹H NMR (400 MHz, CD_2Cl_2) δ 1.24 (d, $J = 6.6$ Hz, 12H, $CHMe_2$), 1.60 (s, 3H, NC(Me)N), 2.17 (s, 18H, η^6-C_6Me_6), 3.33 (sep, $J = 6.6$ Hz, 2H, $CHMe_2$). ¹³C NMR (100 MHz, CD_2Cl_2) δ 14.83 (NC(Me)N), 16.64 (η^6-C_6Me_6), 24.71 ($CHMe_2$), 48.21 ($CHMe_2$), 88.39 (η^6-C_6Me_6), 176.83 (NCN). The ¹³C resonance due to the TfO ligand was not visible. ¹⁹F NMR (376 MHz, CD_2Cl_2) δ −78.95 (s, CF_3).

2a: yield 70%, mp 143 °C (dec). Anal. Calc. for $C_{15}H_{23}N_2O_3F_3SRu$: C, 38.37; H, 4.94; N. 5.97. Found: C, 38.43; H, 5.21; N, 6.03%. ESI-TOF: M−⁻OTf: 321.09. Exact mass (ESI-TOF): Calcd. for $^{12}C_{14}{}^{1}H_{23}{}^{14}N_2{}^{102}Ru_1$: 321.0905. Found: 321.0886. ¹H NMR (400 MHz, CD_2Cl_2) δ 1.22 (d, $J = 6.3$ Hz, 12H, $CHMe_2$), 1.64 (s, 3H, NC(Me)N), 3.32 (sep, $J = 6.3$ Hz, 2H, $CHMe_2$), 5.70 (s, 6H, η^6-C_6H_6). ¹³C NMR (100 MHz, CD_2Cl_2) δ 12.24 (NC(Me)N), 24.42 ($CHMe_2$), 48.00 ($CHMe_2$), 79.71 (η^6-C_6H_6), 160.26 (NCN). The ¹³C resonance due to the TfO ligand was not visible. ¹⁹F NMR (376 MHz, CD_2Cl_2) δ −77.3 (s, CF_3).

2b: yield 82%, mp 145 °C (dec). Anal. Calc. for $C_{20}H_{25}N_2O_3F_3SRu$: C, 45.19; H, 4.74; N. 5.27. Found: C, 45.13; H, 4.79; N, 5.43%. ¹H NMR (600 MHz, CD_2Cl_2) δ 1.12 (br, 12H, $CHMe_2$), 2.97 (sep, $J = 6.2$ Hz, 2H, $CHMe_2$), 5.81 (s, 6H, η^6-C_6H_6), 6.99 (br, 2H, Ph), 7.35 (br, 3H, Ph). ¹³C NMR (150 MHz, CD_2Cl_2) δ 24.41 (br, $CHMe_2$), 48.33 ($CHMe_2$), 79.74 (η^6-C_6H_6), 118.72 (q, $J_{CF} = 319.2$ Hz, CF_3), 126.70 (br, Ph), 128.02, 128.64, 131.78 (Ph), 177.72 (NCN).

2c: mp 200 °C (dec). Anal. Calc. for $C_{22}H_{29}N_2O_3F_3SRu$: C, 47.22; H, 5.22; N. 5.01. Found: C, 47.21; H, 5.22; N, 5.02%. ¹H NMR (400 MHz, CD_2Cl_2) δ 1.09 (s, 18H, $C(CH_3)_3$), 5.82 (s, 6H, η^6-C_6H_6), 7.08 (m, 2H, *ortho*-Ph), 7.23 (m, 2H, *meta*-Ph), 7.32 (m, 1H, *para*-Ph). ¹³C NMR (100 MHz, CD_2Cl_2) δ 32.71 (CMe_3), 55.43 (CMe_3), 80.82 (η^6-C_6H_6), 126.67, 128.35, 129.47, 143.61 (Ph), 163.93 (NCN). The ¹³C resonance due to the TfO ligand was not visible.

4.3. Preparation of $(\eta^6$-$C_6R_6)Ru(X)\{\eta^2$-$R'N{=}C(R'')NR'\}$ (5a-Br, 6a-Br, 6b-Cl, 6c-Cl)

The halogeno complexes, **5a-Br**, **6a-Br**, **6b-Cl**, and **6c-Cl**, were prepared by treatment of Li{R'N=C(R'')NR'}, which was synthesized from R'N=C=NR' with R''Li, with $[(\eta^6$-$C_6Me_6)RuCl_2]_2$ or $[(\eta^6$-$C_6H_6)RuCl_2]_2$. In a typi-

cal example, synthesis of Li{^{i}PrN=C(Ph)N^{i}Pr} was performed by a similar process to that reported for Li{^{t}BuN=C(Ph)N^{t}Bu}. In a Schlenk tube, a cyclohexane–Et_2O solution of PhLi (0.865 M, 6.8 mL, 5.9 mmol) was added to a Et_2O (50 mL) solution of ^{i}PrN=C=N^{i}Pr at 0 °C. The mixture was warmed to room temperature and stirred for 2 h. Removal of solvents in vacuo, the formed air- and moisture sensitive white solids (1.35 g, >99%) were stored in a glove box, and used for the next step without purification. ¹H NMR (400 MHz, THF-d_8) δ 0.88 (br, 12H, $CHMe_2$), 2.96 (br, 2H, $CHMe_2$), 7.04 (br, 2H, Ph), 7.17 (br, 1H, Ph), 7.27 (m, 2H, Ph). ¹³C NMR (100 MHz, CD_2Cl_2) δ 25.32 (br, $CHMe_2$), 67.40 ($CHMe_2$), 126.57 (br, Ph), 127.94, 128.32, 129.03 (Ph). The ¹³C resonance due to the central carbon of the amidinate ligand was not observed. In THF (ca. 20 mL) were dissolved $[(\eta^6$-$C_6H_6)RuCl_2]_2$ (265 mg, 1.06 mmol) and Li{^{i}PrN=C(Ph)N^{i}Pr} (224 mg, 1.07 mmol), and the solution was stirred for 5 h at room temperature. The mixture was concentrated, and the residue was suspended in toluene. After insoluble materials were filtered off, the volatiles were removed in vacuo to form **6b-Cl** as orange solids (354 mg, 79%). The lithium salt, Li{^{i}PrN=C(Me)-N^{i}Pr}, contains substantial amounts of LiBr unless otherwise salt-free MeLi was used. The reaction of Li{^{i}PrN=C(Me)N^{i}Pr} containing LiBr with $[(\eta^6$-$C_6R_6)$-RuCl_2]_2$ was accompanied by halogen exchange of the formed $(\eta^6$-$C_6R_6)Ru(Cl)\{\eta^2$-^{i}PrN=C(R'')N^{i}Pr} to the corresponding bromide, affording **5a-Br** or **6a-Br** as a single product.

$(\eta^6$-$C_6Me_6)Ru(Br)\{\eta^2$-^{i}PrN=C(Me)N^{i}Pr} (**5a-Br**): yield 82%, mp 185 °C (dec). Anal. Calc. for $C_{20}H_{35}N_2BrRu$: C, 49.58; H, 7.28; N. 5.78. Found: C, 49.53; H, 7.31; N, 5.60%. ¹H NMR (400 MHz, C_6D_6) δ 1.21 (d, $J = 6.3$ Hz, 6H, $CHMe_2$), 1.25 (d, $J = 6.3$ Hz, 6H, $CHMe_2$), 1.62 (s, 3H, NC(Me)N), 2.16 (s, 18H, η^6-C_6Me_6), 3.36 (sep, $J = 6.3$ Hz, 2H, $CHMe_2$). ¹³C NMR (100 MHz, C_6D_6) δ 16.48 (NC(Me)N), 17.14 (η^6-C_6Me_6), 24.83 ($CHMe_2$), 26.63 ($CHMe_2$), 48.74 ($CHMe_2$), 88.74 (η^6-C_6Me_6), 174.23 (NCN).

$(\eta^6$-$C_6H_6)Ru(Br)\{\eta^2$-^{i}PrN=C(Me)N^{i}Pr} (**6a-Br**): yield 79%, mp 140 °C (dec). Anal. Calc. for $C_{14}H_{23}N_2BrRu$: C, 42.00; H, 5.79; N. 7.00. Found: C, 41.64; H, 5.79; N, 6.85%. ¹H NMR (400 MHz, C_6D_6) δ 1.13 (d, $J = 6.1$ Hz, 6H, $CHMe_2$), 1.33 (s, 3H, NC(Me)N), 1.39 (d, $J = 6.1$ Hz, 6H, $CHMe_2$), 3.31 (sep, $J = 6.1$ Hz, 2H, $CHMe_2$), 4.90 (s, 6H, η^6-C_6H_6). ¹³C NMR (100 MHz, C_6D_6) δ 13.22 (NC(Me)N), 25.87 ($CHMe_2$), 26.19 ($CHMe_2$), 48.27 ($CHMe_2$), 81.03 (η^6-C_6H_6), 172.94 (NCN).

$(\eta^6$-$C_6H_6)Ru(Cl)\{\eta^2$-^{i}PrN=C(Ph)N^{i}Pr} (**6b-Cl**): mp 210 °C (dec). Anal. Calc. for $C_{20}H_{25}N_2ClRu$: C, 54.60; H, 6.03; N. 6.70. Found: C, 54.26; H, 6.07; N, 6.68%. ¹H NMR (400 MHz, C_6D_6) δ 1.12 (d, $J = 6.4$ Hz, 6H, $CHMe_2$), 1.16 (d, $J = 6.4$ Hz, 6H, $CHMe_2$), 3.05 (sep, $J = 6.4$ Hz, 2H, $CHMe_2$), 5.61 (s, 6H, η^6-C_6H_6), 7.09 (br, 1H, Ph), 7.17 (br, 1H, Ph), 7.32 (br, 3H, Ph). ¹³C NMR (100 MHz, C_6D_6) δ 25.23 ($CHMe_2$), 26.83 ($CHMe_2$),

48.56 ($CHMe_2$), 81.14 (η^6-C_6H_6), 127.60 (br), 127.93, 128.51, 128.80 (br), 132.95 (Ph), 175.93 (NCN).

(η^6-C_6H_6)Ru(Cl){η^2-^tBuN=$C(Ph)N^tBu$} (**6c-Cl**): yield 57%, mp 220 °C (dec). Anal. Calc. for $C_{21}H_{29}N_2ClRu$: C, 56.55; H, 6.55; N. 6.28. Found: C, 56.21; H, 6.61; N, 6.00%. ^1H NMR (400 MHz, C_6D_6) δ 1.26 (s, 18H, ^tBu), 5.02 (s, 6H, η^6-C_6H_6), 6.94–7.08 (m, 3H, Ph), 7.11 (m, 1H, Ph), 7.49 (m, 1H, Ph). ^{13}C NMR (100 MHz, C_6D_6) δ 34.11 (CMe_3), 55.82 (CMe_3), 82.01 (η^6-C_6H_6), 126.96, 126.97, 128.42, 129.67, 132.09, 143.61 (Ph), 174.51 (NCN).

4.4. Preparation of [(η^5-C_5Me_5)Ru(μ-η^2-^iPrN=$C(Me)N$-^iPr)Ru(κ-OTf)(η^5-C_5R_5)] (3; R = Me; 4; R = H)

Preparation of [(η^5-C_5Me_5)Ru(μ-η^2-^iPrN=$C(Me)N^iPr$)-Ru(η-X)(η^5-C_5R_5)] was reported previously. In a Schlenk tube were placed [(η^5-C_5Me_5)Ru(μ-η^2-^iPrN=$C(Me)N^iPr$)-Ru(η-Br)(η^5-C_5Me_5)] (200 mg, 0.288 mmol) and AgOTf (150 mg, 0.583 mmol), and CH_2Cl_2 (5 mL) was added. The suspension was stirred for 1 h at room temperature. After removal of the silver salt by filtration, the filtrate was concentrated in vacuo. The residue was recrystallized from a mixture of CH_2Cl_2 and pentane to give **3** as purple crystals in 92% yield (203 mg). Similar treatment of

[(η^5-C_5Me_5)Ru(μ-η^2-^iPrN=$C(Me)N^iPr$)Ru(η-Cl)(η^5-C_5H_5)] (100 mg, 0.173 mmol) with TlOTf (100 mg, 0.282 mmol) in CH_2Cl_2 (5 mL) afforded **4** as red crystals in 90% yield (108 mg).

3: mp 142 °C (dec). Anal. Calc. for $C_{29}H_{47}F_3N_2O_3Ru_2S$: C, 45.66; H, 6.27; N, 3.67. Found: C, 45.22; H, 6.12; N, 3.60%. ESI-TOF: M$-^-$OTf: 615.18. Exact mass (ESI-TOF): Calcd. for $^{12}C_{28}{}^1H_{47}{}^{14}N_2{}^{102}Ru_2$: 615.1826. Found 615.1838. ^1H NMR (600 MHz, CD_2Cl_2) δ 1.58 (s, 3H, NC(Me)N), 1.59 (s, 30H, C_5Me_5), 1.61 (d, J = 6.6 Hz, 12H, $CHMe_2$), 3.26 (sep, J = 6.6 Hz, 2H, CHMe$_2$). ^{13}C NMR (150 MHz, CD_2Cl_2) δ 11.9 (C_5Me_5), 15.1 (NC(Me)N), 24.3 ($CHMe_2$), 54.6 ($CHMe_2$), 82.2 (C_5Me_5), 124.4 (NCN). ^{19}F NMR (565 MHz, CD_2Cl_2) δ −79.0. IR (KBr, cm^{-1}) 1296, 1230.

4: mp 142 °C (dec). Anal. Calc. for $C_{24}H_{37}F_3N_2O_3Ru_2S$: C, 41.61; H, 5.38; N, 4.04. Found: C, 41.36; H, 5.31; N, 3.99%. ESI-TOF: M$-^-$OTf: 545.10. Exact mass (ESI-TOF): Calcd. for $^{12}C_{23}{}^1H_{37}{}^{14}N_2{}^{102}Ru_2$: 545.1044. Found 545.1036. ^1H NMR (600 MHz, CD_2Cl_2) δ 1.06 (d, J = 6.6 Hz, 6H, $CHMe_2$), 1.26 (d, J = 6.6 Hz, 6 H, $CHMe_2$), 1.65 (s, 15 H, C_5Me_5), 1.91 (s, 3 H, NC(Me)N), 2.86 (sep. J = 6.6 Hz, 2H, CHMe$_2$), 4.44 (s, 5 H, C_5H_5). ^{13}C NMR (150 MHz, CD_2Cl_2) δ 10.3 (C_5Me_5), 15.7

Table 4
Crystallographic tables

	1	**2c**	**3**	**4**
Empirical formula	$C_{21}H_{35}F_3O_3RuSN_2$	$C_{22}H_{29}F_3O_3RuSN_2$	$C_{29}H_{47}N_2O_3F_3Ru_2S$	$C_{24}H_{37}F_3N_2O_3Ru_2S$
Crystal size (mm)	$0.20 \times 0.20 \times 0.20$	$0.35 \times 0.20 \times 0.20$	$0.30 \times 0.30 \times 0.10$	$0.20 \times 0.03 \times 0.02$
Crystal color, habit	Orange, block	Red, prismatic	Red prism	Red, platelet
Formula weight	553.64	559.61	762.90	692.76
Temperature (K)	123(2)	293(2)	123(2)	123(2)
Radiation	Mo Kα (0.71069 Å)	Mo Kα (0.71069 Å)	Mo Kα (0.71069 Å)	Mo Kα (0.71069 Å)
Crystal system	Orthorhombic	Orthorhombic	Monoclinic	Orthorhombic
Space group	$Pbca$ (#61)	$Pnma$ (#62)	$P2_1/c$ (#14)	$Pna2_1$ (#33)
Unit cell parameters				
a (Å)	15.950(4)	18.830(4)	10.6176(2)	14.176(2)
b (Å)	15.311(4)	10.799(2)	15.9728(3)	18.841(2)
c (Å)	19.471(5)	12.005(3)	19.0453(4)	10.2680(13)
α(°)	90	90	90	90
β (°)	90	90	101.9811(8)	90
γ (°)	90	90	90	90
V (Å^3)	4755.2(19)	2441.1(9)	3159.6(1)	2742.5(6)
Z	8	4	4	4
ρ_{calc} (g cm^{-3})	1.547	1.523	1.604	1.678
μ(Mo Kα) (cm^{-1})	7.95	7.76	10.72	12.26
$F(000)$	2288.00	1144.00	1560.00	1400.00
θ Range (°)	3.1–27.5	2.54–27.49	2.3–27.5	3.1–27.5
No. observations	5441 ($I > 0.00\sigma(I)$)	1876($I > 2.00\sigma(I)$)	7216 ($I > 0.00\sigma(I)$)	6254 ($I > 0.00\sigma(I)$)
No. variables	315	166	408	354
Reflection/parameter ratio	17.27	11.30	17.69	17.67
R (all reflections)	0.109	0.097	0.043	0.034
$R_1(I > 2.00\sigma(I))$[a]	0.054	0.048	0.033	0.029
wR_2 (all reflections)[b]	0.127	0.146	0.096	0.063
GOF	1.000	1.019	1.000	1.008
Flack parameter	–	–	–	0.00(3) (Friedel pairs = 2494)
Max shift/error in final cycle	0.000	0.000	0.000	0.000
Maximum peak in final diff. map (e$^-$/Å^3)	1.94	0.57	0.76	1.55
Minimum peak in final diff. map (e$^-$/Å^3)	−1.02	−0.697	−0.70	−0.95

[a] $R_1 = \sum|F_o| - |F_c|/\sum|F_o|$.
[b] $wR_2 = [\sum(w(F_o^2 - F_c^2)^2)/\sum(w(F_o^2)^2)]^{1/2}$.

(NC(*Me*)N), 21.5 and 25.8 (CH*Me*$_2$), 52.6 (*C*HMe$_2$), 66.3 (*C*$_5$H$_5$), 82.2 (*C*$_5$Me$_5$), 129.8 (NCN). ^{19}F NMR (565 MHz, CD$_2$Cl$_2$) δ −78.0. IR (KBr, cm^{-1}) 1285, 1260.

4.5. Reactions of $(\eta^6\text{-}C_6H_6)Ru(X)\{\eta^2\text{-}^tBuN{=}C(Ph)N^tBu\}$ (6c-Br: X = Br, 2c: X = OTf) with auxiliary ligands

Reactions of $[(\eta^6\text{-}C_6H_6)Ru\{\eta^2\text{-}^tBuN{=}C(Ph)N^tBu\}]^+$-(TFPB)$^-$ (**7**) with PPh$_3$, pyridine, ^{t}BuNC, CO, and CH$_2$=CH$_2$ were reported elsewhere. The bromide **6c-Br** reacted with ^{t}BuNC to give the corresponding adduct **10-Br**, whereas formation of the PPh$_3$ adduct **8-Br** was detected by NMR. The triflate **2c** reacted with PPh$_3$, pyridine and ^{t}BuNC to afford the corresponding adduct, **8-OTf**, **9-OTf**, and **10-OTf**, respectively. All of the reactions were performed in a similar fashion, and a typical example is as follows: In CH$_2$Cl$_2$ (5 mL) were dissolved **2c** (34 mg, 0.061 mmol) and PPh$_3$ (17 mg, 0.065 mmol) at −78 °C. The mixture was slowly warmed to room temperature and stirred for 1 h. Removal of the solvent in vacuo, and the formed crude product was recrystallized from CH$_2$Cl$_2$/pentane at −35 °C to give **8-OTf** (47 mg) in 94% yield.

8-OTf: mp. 180 °C (dec). Anal. Calc. for C$_{40}$H$_{44}$-N$_2$O$_3$F$_3$P$_1$SRu: C, 58.45; H, 5.40; N, 3.41. Found: C, 58.03; H, 5.36; H, 3.29%. ^{1}H NMR (400 MHz, CDCl$_3$) δ 0.83 (s, 18H, ^{t}Bu), 6.04 (s, 6H, η^6-C$_6$H$_6$), 7.29–7.32 (m, 2H, Ph), 7.37–7.47 (m, 9H, Ph), 7.51–7.60 (m, 9H, Ph). ^{13}C NMR (100 MHz, CDCl$_3$) δ 30.32 (C*Me*$_3$), 55.20 (*C*Me$_3$), 89.83 (d, $J_{C\text{-}P}$ = 2.9 Hz, η^6-C$_6$H$_6$), 126.99, 127.61, 127.89 (d, $J_{C\text{-}P}$ = 1.2 Hz), 128.93, 128.98 (d, $J_{C\text{-}P}$ = 9.9 Hz), 129.49, 131.35 (br), 131.64, 133.52 (d, $J_{C\text{-}P}$ = 9.9 Hz), and 138.13 (d, $J_{C\text{-}P}$ = 2.5 Hz) (Ph), 171.48 (d, $J_{C\text{-}P}$ = 3.7 Hz, NCN). ^{31}P NMR (162 MHz, CDCl$_3$) δ 28.03 (PPh$_3$).

9-OTf: yield 82%. mp. 180 °C (dec). Anal. Calc. for C$_{27}$H$_{34}$N$_3$O$_3$F$_3$SRu: C, 50.77; H, 5.37; N, 6.58. Found: C, 50.60; H, 5.39; H, 6.53%. ^{1}H NMR (400 MHz, CDCl$_3$) δ 0.97 (s, 18H, ^{t}Bu), 6.00 (s, 6H, η^6-C$_6$H$_6$), 6.72 (m, 1H, Ph), 7.16–7.25 (m, 2H, Ph), 7.31–7.39 (m, 2H, Ph), 7.62 (ddd, J = 7.6, 6.6, 1.5 Hz, 2H, C$_5$H$_5$N), 7.95 (tt, J = 7.6, 1.5 Hz, 1H, C$_5$H$_5$N), 9.09 (dd, J = 6.6, 1.5 Hz, 2H). ^{13}C NMR (150 MHz, CDCl$_3$) δ 30.34 (C*Me*$_3$), 55.28 (*C*Me$_3$), 84.71 (η^6-C$_6$H$_6$), 126.18 (C$_5$H$_5$N), 127.25, 127.82, 128.98, 129.36, 129.50, and 138.16 (Ph), 139.13, 154.88 (C$_5$H$_5$N), 171.50 (s, NCN).

10-OTf: yield 89%. mp. 140 °C (dec). Anal. Calc. for C$_{27}$H$_{38}$N$_3$O$_3$F$_3$SRu: C, 50.45; H, 5.96; N, 6.54. Found: C, 49.97; H, 5.83; H, 6.47%. ^{1}H NMR (400 MHz, CDCl$_3$) δ 0.94 (s, 18H, C*Me*$_3$ of the amidinate), 1.68 (s, C*Me*$_3$ of the isocyanide), 6.12 (s, 6H, η^6-C$_6$H$_6$), 7.19–7.30 (m, 2H, Ph), 7.33 (m, 2H, Ph), 7.39 (m, 1H, Ph). ^{13}C NMR (150 MHz, CDCl$_3$) δ 30.49 (C*Me*$_3$ of the isocyanide), 33.26 (C*Me*$_3$ of the amidinate), 55.38 (*C*Me$_3$ of the amidinate), 84.71 (η^6-C$_6$H$_6$), 127.19, 128.012, 129.09, 129.36, 130.030, and 138.34 (Ph), 172.61 (NCN). The ^{13}C resonance due to the TfO, C*Me*$_3$ of the isocyanide, *C*N of the isocyanide were not visible. IR (KBr, cm^{-1}) 2135.

4.6. X-ray data collection and reduction

Single crystals of **1a**, **2c**, **3**, **4**, **9-OTf**, **10-OTf** were grown from CH$_2$Cl$_2$/pentane. X-ray crystallography were performed on a Rigaku Saturn CCD area detector in the case of **1a** and **4**, and on a Rigaku RAXIS RAPID imaging plate diffraction meter in the case of **2c**, **3**, **9-OTf** and **10-OTf** with graphite monochromated Mo Kα radiation (λ = 0.71070A). The data were collected at 123(2) K for **1a**, **3** and **4**, 223(2) K for **9-OTf** and **10-OTf**, and 293(2) K for **2c**. The data were corrected for Lorentz and polarization effects. The structures were solved by direct methods (SIR92) [8] in the case of **2c** and **9-OTf**, by direct method (SIR97) [9] in the case of **1a**, by Patterson method (DIRDIF94 PATTY) [10] for **10-OTf**, and by Patterson method (DIRDIF 99 PATTY) [11] in the case of **3** and **4**, and expanded using Fourier techniques [12]. The non-hydrogen atoms were refined anisotropically. Hydrogen atoms were refined using the riding model. The final cycle of full-matrix least-squares refinement on F^2 was based on 5441 observed reflections and 315 variable parameters for **1a**, 1876 observed reflections and 166 variable parameters for **2c**, 7216 observed reflections and 408 variable parameters for **3**, 6254 observed reflections and 354 variable parameters

Table 5
Crystallographic tables

	9-OTf	10-OTf
Empirical formula	C$_{27}$H$_{34}$F$_3$N$_3$O$_3$RuS	C$_{27}$H$_{38}$O$_3$N$_3$F$_3$SRu
Crystal size (mm)	0.35 × 0.13 × 0.08	0.30 × 0.20 × 0.10
Crystal color, habit	Yellow, plate	Yellow, prism
Formula weight	638.71	642.73
Temperature (K)	223(2)	223(2)
Radiation	Mo Kα (0.71069 Å)	Mo Kα (0.71069 Å)
Crystal system	Triclinic	Monoclinic
Space group	$P\bar{1}$ (#2)	$P2_1/n$ (#14)
Unit cell parameters		
a (Å)	10.719(2)	9.4434(2)
b (Å)	16.148(3)	29.0548(7)
c (Å)	8.892(2)	11.3224(3)
α (°)	103.95(1)	90
β (°)	94.38(2)	98.9770(4)
γ (°)	71.84(1)	90
V (Å^3)	1419.3(5)	3068.5(1)
Z	2	4
ρ_{calc} (g cm^{-3})	1.494	1.391
μ (Mo Kα) (cm^{-1})	6.79	6.28
$F(000)$	656.00	1328.00
θ Range (°)	2.73–27.50	2.59–27.48
No. observations	3978 ($I > 3.00\sigma(I)$)	4063 ($I > 3.00\sigma(I)$)
No. variables	343	343
Reflection/parameter ratio	11.60	11.85
$R_1(I > 3.00\sigma(I))^a$	0.045	0.050
wR_2 (all reflections)^b	0.109	0.155
GOF	1.007	0.87
Max shift/error in final cycle	0.001	0.000
Maximum peak in final diff. map (e$^-$/Å^3)	1.26	0.41
Minimum peak in final diff. map (e$^-$/Å^3)	−0.85	−0.47

^{a} $R_1 = \sum|F_0| - |F_c|/\sum|F_0|$.
^{b} $wR_2 = [\sum(w(F_o^2 - F_c^2)^2)/\sum(w(F_o^2)^2)]^{1/2}$.

for **4**, 3978 observed reflections and 343 variable parameters for **9-OTf**, 4063 observed reflections and 343 variable parameters for **10-OTf**. Neutral atom scattering factors were taken from Cromer and Waber [13]. All calculations were performed using the CrystalStructure [14,15] crystallographic software package for **1a** and **4**, and all calculations for **2c**, **3**, **9-OTf** and **10-OTf** were performed using the teXsan [16] crystallographic software package of Molecular Structure Corporation except for refinement, which was performed using SHELXL-97 [17]. Details of final refinement are summarized in Tables 4 and 5, and the numbering scheme employed is shown in Figs. 3 and 6, which was drawn with ORTEP at 50% probability ellipsoid. Detailed data as well as the bond distances and angles are shown in Supporting information.

Acknowledgements

Appendix A. Supplementary data

The CIF files for the compound **1a**, **2c**, **3**, **4**, **9-OTf** and **10-OTf**, ^1H and ^{13}C spectra of **1a**, **2a**, **2c**, **3**, **4**, **6-Cl**, **9-OTf** and **10-OTf**, variable temperature ^1H and ^{19}F NMR data of **1a**, **2a**, **3** and **4**, and ESI mass spectra of **1a**, **2a**, **3** and **4**. Supplementary data associated with this article can be found, in the online version, at doi:10.1016/j.jorganchem.2006.08.069.

References

[1] For reviews: (a) G.A. Lawrance, Chem. Rev. 86 (1986) 17;
(b) W. Beck, K. Sünkel, Chem. Rev. 88 (1988) 1405;
(c) S.H. Strauss, Chem. Rev. 93 (1993) 927.

[2] For a review: E.Y.-X. Chen, T. Marks, Chem. Rev. 100 (2000) 1391.

[3] (a) D.A. Evans, J.A. Murry, P. von Matt, R.D. Norcross, S. Miller, Angew. Chem., Int. Ed. Engl. 34 (1995) 798;
(b) E.P. Kundig, C.M. Saudan, G. Bernardinelli, Angew. Chem., Int. Ed. Engl. 38 (1999) 1219.

[4] (a) M.J.A. Kraakman, B. de Klerk-Engels, P.P.M. de Lange, K. Vrieze, W.J. Smeets, A.L. Spek, Organometallics 11 (1992) 3774;
(b) P.W. Blosser, J.C. Gallucci, A. Wojcicki, Inorg. Chem. 31 (1992) 2376;
(c) B. de Klerk-Engels, J.H. Groen, M.J.A. Kraakman, J.M. Ernsting, K. Vrieze, K. Goubitz, J. Fraanje, Organometallics 13 (1994) 3279;
(d) R.M. Barns, J.L. Hubbard, J. Am. Chem. Soc. 116 (1994) 9514;
(e) J.-P. Sutter, S.L. James, P. Steenwinkel, T. Karlen, D.M. Grove, N. Veldman, W.J.J. Smeets, A.L. Spek, G. van Koten, Organometallics 15 (1996) 941;
(f) A. Svetlanova-Larsen, C.R. Zoch, J.L. Hubbard, Organometallics 15 (1966) 3076;
(g) C. Gemel, D. Kalt, K. Mareiter, V.N. Sapunov, R. Schmid, K. Kirchner, Organometallics 16 (1997) 427;
(h) A.C. Ontko, J.F. Houlis, R.C. Schnabel, D.M. Roddick, T.P. Fong, A.J. Lough, R.H. Morris, Organometallics 17 (1998) 5467;
(i) R.A.T.M. Abbenhuis, I. del Río, M.M. Bergshoef, J. Boersma, N. Veldman, A.L. Spek, G. van Koten, Inorg. Chem. 37 (1998) 1749;
(j) T. Funaioli, C. Cavazza, F. Marchetti, G. Fachinetti, Inorg. Chem. 38 (1999) 3361;
(k) I. del Río, R.A. Gossage, M.S. Hannu, M. Lutz, A.L. Spek, G. van Koten, Organometallics 18 (1999) 1097;
(l) T.P. Fong, C.E. Forde, A.L. Lough, R.H. Morris, P. Rigo, E. Rocchini, T. Stephan, J. Chem. Soc., Dalton Trans. (1999) 4475;
(m) C.J. den Reijer, M. Wörle, P.S. Pregosin, Organometallics 19 (2000) 309;
(n) D. Huang, J.C. Bollinger, W.E. Streib, K. Folting, V. Young Jr., O. Eisenstein, K.G. Caulton, Organometallics 19 (2000) 2281;
(o) C.P. Casey, T.E. Vos, S.W. Singer, I.G. Guzei, Organometallics 21 (2002) 5038;
(p) M.D. Hagereaves, M.F. Mahon, M.K. Whittlesey, Inorg. Chem. 41 (2002) 3137;
(q) M.A.O. Volland, S.M. Hansen, F. Rominger, P. Hofmann, Organometallics 23 (2004) 800;
(r) J.M. Bikley, A.A. La Pensee, S.J. Higgins, C.A. Stuart, Dalton Trans. (2003) 4663;
(s) J.O. Krause, O. Nuyken, K. Wurst, M.R. Buchmeiser, Chem. Eur. J. 10 (2004) 777;
(t) F.A. Cotton, C.A. Murillo, J.H. Reinbenspies, D. Villagrán, X. Wang, C.C. Wilkinson, Inorg. Chem. 43 (2004) 8373.

[5] (a) Y. Yamaguchi, H. Nagashima, Organometallics 19 (2000) 725;
(b) T. Hayashida, Y. Yamaguchi, K. Kirchner, H. Nagashima, Chem. Lett. (2001) 954;
(c) H. Kondo, H. Nagashima, J. Am. Chem. Soc. 123 (2001) 500;
(d) H. Kondo, K. Matsubara, H. Nagashima, J. Am. Chem. Soc. 124 (2002) 534;
(e) J. Terasawa, H. Kondo, T. Matsumoto, K. Kirchner, Y. Motoyama, H. Nagashima, Organometallics 24 (2005) 2713;
(f) For an account: H. Nagashima, H. Kondo, T. Hayashida, Y. Yamaguchi, M. Gondo, S. Masuda, K. Miyazaki, K. Matsubara, K. Kirchner, Coord. Chem. Rev. 245 (2003) 177;
(g) Application to catalysis: Y. Motoyama, M. Gondo, S. Masuda, Y. Iwashita, H. Nagashima, Chem. Lett. 33 (2004) 442;
(h) Application to catalysis: Y. Motoyama, S. Hanada, S. Niibayashi, K. Shimamoto, N. Takaoka, H. Nagashima, Tetrahedron 61 (2005) 10216.

[6] (a) T. Hayashida, H. Nagashima, Organometallics 21 (2002) 3884;
(b) T. Hayashida, H. Nagashima, The Reports of Institute of Advanced Material Study, Kyushu University, vol. 15, 2000, p. 31;
(c) Crystal structures and reactions of several other (η^6-arene)Ru(η^2-amidinate)X complexes were investigated; T. Hayashida, H. Nagashima, unpublished results.

[7] For a related guanizine complex: (a) P.J. Bailey, L.A. Mitchel, S. Parsons, J. Chem. Soc., Dalton Trans. (1996) 2839;
(b) P.J. Bailey, K.J. Grant, L.A. Mitchel, S. Pace, A. Parkin, S. Parsons, J. Chem. Soc., Dalton Trans. (2000) 1987.

[8] SIR92: A. Altomare, M. Cascarano, C. Giacovazzo, A. Guagliardi, J. Appl. Crystallogr. 26 (1993) 343.

[9] SIR 97 A. Altomare, M. Burla, M. Camalli, M. Cascarano, C. Giacovazzo, A. Guagliardi, A. Moliterni, G. Polidori, R. Spagna, J. Appl. Crystallogr. 32 (1999) 115.

[10] DIRDIF94: P.T. Beurskens, G. Admiraal, G. Beurskens, W.P. Bosman, S. Garcia-Granda, R.O. Gould, J.M.M. Smits, C. Smykalla, The DIRDIF-94 program system; Technical Report of the Crystallography Laboratory, University of Nijmegen, Nijmegen, The Netherlands, 1992.

[11] DIRDIF99: P.T. Beurskens, G. Admiraal, G. Beurskens, W.P. Bosman, R. de Gelder, R. Israel, J.M.M. Smits, The DIRDIF-99 program system, Technical Report of the Crystallography Laboratory, University of Nijmegen, Nijmegen, The Netherlands, 1999.

[12] PATTY: P.T. Beurskens, G. Admiraal, G. Beurskens, W.P. Bosman, S. Garcia-Granda, R.O. Gould, J.M.M. Smits, C. Smykalla, The DIRDIF program system, Technical Report of the Crystallography Laboratory, University of Nijmegen, Nijmegen, The Netherlands, 1992.

[13] D.T. Cromer, J.T. WaberInternational Tables for X-ray Crystallography, vol. 4, Kynoch Press, Birmingham, UK, 1974.

[14] CrystalStructure 3.6.0: Crystal Structure Analysis Package, Package, Rigaku and Rigaku/MSC, 9009 New Trails Dr. The Woodlands, TX 7738,1 USA, 2000–2004.

[15] CRYSTALS Issue 10: D.J. Watkin, C.K. Prout, J.R. Carruthers, P.W. Betteridge, Chemical Crystallography Laboratory, Oxford, UK, 1996.

[16] teXsan for Windows: Crystal Structure Analysis Package, Molecular Structure Corporation, 1997.

[17] SHELX97: G.M. Sheldrick, 1997.